



HAL
open science

Ruthenium tris(2,2'-bipyridyl) complex encapsulated in nanosized faujasite zeolite as intracellular localization tracer

Sarah Komaty, Hayriye Özçelik, Moussa Zaarour, Aurélie Ferré, Samuel Valable, Svetlana Mintova

► To cite this version:

Sarah Komaty, Hayriye Özçelik, Moussa Zaarour, Aurélie Ferré, Samuel Valable, et al.. Ruthenium tris(2,2'-bipyridyl) complex encapsulated in nanosized faujasite zeolite as intracellular localization tracer. *Journal of Colloid and Interface Science*, 2020, 581 (Part B), pp.919-927. 10.1016/j.jcis.2020.08.117 . hal-02935419

HAL Id: hal-02935419

<https://normandie-univ.hal.science/hal-02935419v1>

Submitted on 27 Nov 2020

HAL is a multi-disciplinary open access archive for the deposit and dissemination of scientific research documents, whether they are published or not. The documents may come from teaching and research institutions in France or abroad, or from public or private research centers.

L'archive ouverte pluridisciplinaire **HAL**, est destinée au dépôt et à la diffusion de documents scientifiques de niveau recherche, publiés ou non, émanant des établissements d'enseignement et de recherche français ou étrangers, des laboratoires publics ou privés.

Ruthenium tris bipyridyl complex encapsulated in nanosized FAU zeolite as intracellular localization tracer

Sarah Komaty,^{a,#} Hayriye Özçelik,^{b,#} Moussa Zaarour,^a Aurélie Ferre,^b Samuel Valable,^{b,*} Svetlana Mintova^{a,*}

^a Normandie Univ., UNICAEN, CNRS, ENSICAEN, Laboratoire Catalyse et Spectrochimie (LCS), 14050 Caen, France.

^bImagerie et Stratégies Thérapeutiques des pathologies Cérébrales et Tumorales, CERVOxy Group, CNRS, CEA, 14050 Caen, France.

These authors contributed equally to this work

* Correspondence: svetlana.mintova@ensicaen.fr; samuel.valable@cnrs.fr

ABSTRACT

Designing zeolites for medical applications is a challenging task requiring the introduction of new functionalities without altering their intrinsic properties such as morphology, crystallinity, colloidal stability, surface charge, and porosity. Herein, we present the encapsulation of luminescent ruthenium-tris(2,2'-bipyridyl) complex in FAU zeolite nanocrystals (Ru(bpy)₃-FAU) and their use as an intracellular localization tracer. Upon exciting of the Ru(bpy)₃-FAU zeolite at 450 nm, the sample gives rise to an orange-red emission at 628 nm thus permitting its use for cellular imaging and localization of the zeolite nanoparticles. The nanosized Ru(bpy)₃-FAU zeolite is characterized in terms of size, charge, crystallinity, morphology, porosity, thermal stability, and sorption capacity. The potential toxicity of Ru(bpy)₃-FAU on U251-MG

glioblastoma cells was evaluated. A safe concentration (50-100 $\mu\text{g/ml}$) for the $\text{Ru}(\text{bpy})_3\text{-FAU}$ zeolite is identified. The luminescent properties of the ruthenium complex confined in the zeolite nanocrystals allow to detect their localization in the U251-MG cells with a main accumulation in the cytoplasm. The $\text{Ru}(\text{bpy})_3\text{-FAU}$ nanosized zeolite is a potential candidate for biological applications for being stable, safe, capable of loading respiratory gases, and easily probed in the cells owing to its luminescent properties.

Keywords

Zeolites, nanocrystals, encapsulation, luminescence, intracellular tracer, cell uptake, cytotoxicity.

INTRODUCTION

Zeolites are crystalline microporous aluminosilicates with large surface area, and well-defined pores and cages. The size and shape of their pores and cages are the base for the selective gas sieving and discrimination of guest molecules. They allow ions and compounds with smaller dimensions than the zeolite pore apertures to diffuse into the internal voids, whereas they restrict the access for bigger compounds and complexes. The zeolite internal voids are usually occupied with charge compensating cations and water molecules; these can be exchanged for other cations or partially replaced with appropriate adsorbing compounds.¹ The admissibility of zeolites for various applications is linked to their modifiable chemical composition, high porous character, exchangeable charge compensating cations, variable hydrophilicity/hydrophobicity, and controlled adsorption properties. Recently, more attention was given to the use of zeolites in biomedical applications² as antimicrobial agents,^{3,4} anti-cancer drugs carriers,⁵ and in the storage and controlled delivery of drugs and gases.⁶⁻⁸ More specifically, they were considered as carriers

for the delivery of anti-neoplastic compounds,⁹⁻¹¹ nucleic acids,^{12,13} both hydrophilic^{14,15} and lipophilic drugs,^{9,16} anti-inflammatory drugs,¹⁷ and also for the delivery of gases that could be of interest in the biomedical field.^{7,18} Faujasite nanozeolite is a potential candidate for biomedical applications due to its large surface area, high micropore volume, and the presence of supercage (1.2 nm) that can host different drugs^{19,20} or gases.⁸

Besides, zeolites modified with luminescent metal clusters,²¹ lanthanides,²² and metal complexes²³ were also used to upgrade their properties especially for optical oxygen sensors application. Confining luminescent compounds within the zeolites limits the formation of chromophore aggregates. Consequently, partial or complete loss of emission through nonradiative pathways²⁴ is eliminated, and the luminescent properties are enhanced.^{25,26} Numerous nanoparticles enter inside the cells through a process termed "endocytosis". The particles immersed in membrane-bound vesicles are also known as endosomes (or phagosomes in case of phagocytosis),^{27,28} which are pinched off membrane invaginations. Then the cargo is sorted through vesicles to various intracellular compartments or nuclei and recycled to extracellular environment.^{27,28} There, the guest molecule would allow monitoring the exact location of the nanoparticles (zeolites or others) owing to their luminescent properties. Most studies of the cellular uptake and tracing of nanoparticles have been performed using luminescent labelled nanoparticles.²⁹ Experiments revealed several problems associated with such systems, especially in the case of organic dyes; photodecomposition, insolubility in the hydrophobic support matrices, and leaching from the zeolite support are often observed. A solution to these problems is to confine a luminescent molecule such as ruthenium-tris(2,2'-bipyridyl) within zeolite nanoparticles, for example in the supercages of Faujasite (FAU) zeolite. The diameter of the ruthenium-tris(2,2'-bipyridyl) complex is 12 Å, which is comparable to the

size of the supercage of FAU. However, the diameter of the ruthenium-tris(2,2'-bipyridyl) complex is by far larger than the pore opening of zeolite (7.4 Å), thus cannot leach out of the pores.³⁰ The use of modified FAU as optical sensor was reported in literature.³¹ Additionally, the migration of oxygen within zeolite by studying its emission quenching,³² and detection of dissolved oxygen in aqueous media were also reported.^{21,23}

Herein, we present the incorporation of ruthenium-tris(2,2'-bipyridyl) complex in nanosized FAU zeolite crystals with a particle size in the range of 20-30 nm (sample Ru(bpy)₃-FAU). The nanosized FAU zeolite containing the ruthenium complex, due to the optical properties inherited from the luminescent ruthenium complex is used as an intracellular localization tracer. The cytotoxicity tests of Ru(bpy)₃-FAU for eukaryotic cells reveal that it is safe in the concentration range of 50-100 µg/ml. Due to its small dimensions, the modified zeolite crystals are capable of crossing the cell membrane barrier and residing in the cytoplasm. Owing to all these features, we believe that the Ru(bpy)₃-FAU nanocrystals can be used as a safe intracellular localization tracer and active carrier for various biomedical uses.

Experimental part

Materials: Al powder (Al, 325 mesh, 99.5%, Alfa Aesar, Karlsruhe, Germany), sodium hydroxide (NaOH, 97%, Sigma-Aldrich, Lyon, France), colloidal silica (SiO₂, Ludox HS-30, 30 wt % SiO₂, pH = 9.8, Sigma-Aldrich, Lyon, France), ruthenium chloride (99.9% (PGM basis), Ru 38% min, Alfa Aesar, Karlsruhe, Germany), 2,2'-dipyridyl (99+ %, Acros Organics), N,N-dimethylformamide (DMF, 99.8+%, Alfa Aesar, Karlsruhe, Germany), lithium chloride, (99+%, Thermo Fisher Scientific, Geel, Belgium), acetonitrile anhydrous (ACROS Organics), ethanol

absolute (Sigma-Aldrich, Lyon, France), and diethyl ether (99 +%, ACROS Organics) were used as received.

A human glioblastoma cell line, U251-MG was purchased from American Type Culture Collections (ATCC, Manassas, VA, USA). Dulbecco's Modified Eagle Medium (DMEM), (Low Glucose), penicillin/streptomycin (10,000 units), trypsin-EDTA (0.25%), glutamine, Paraformaldehyde, Hoechst 33342 (10 µg/ml) were purchased from Sigma, France.

Preparation of zeolite X (sample FAU): The nanosized FAU zeolite in sodium form free of organic template (20-30 nm) with Si / Al = 1.2 was-prepared following an original reported procedure by our group.³³

Encapsulation of ruthenium-tris(2,2'-bipyridyl) in nanosized FAU zeolite (sample Ru(bpy)₃-FAU): Ru(bpy)₃-FAU was-prepared by following a reported procedure after modification.²⁴ One molar equivalence (1 eq) of RuCl₃ (0.128g), 2 eq of LiCl (0.06 g), and 1 eq of 2,2'-bipyridyl (0.096 g) were introduced into 5 mL of DMF. The solution was heated under stirring at 90 °C for 7 h and then left to cool down to room temperature. The obtained product was purified by crystallization in diethyl ether, dissolved in CH₃CN, and then passed over Büchner funnel to eliminate LiCl. The obtained red solution was added under N₂ atmosphere to 300 mg of FAU readily preheated at 200 °C under vacuum for 2 h; the resulting suspension was stirred for 18 h at room temperature. At the end of the reaction, the powder was collected by centrifugation (20000 rpm, 30 min) and washed several times with acetonitrile until the supernatant became colorless. The collected brownish zeolite was dispersed in 50 mL of ethanol, and then an excess of the ligand 2,2'-bipyridyl (0.528 g) was introduced. The mixture was refluxed for two days during which the color evolved from green to brownish -red to orange. The

product was separated by centrifugation, washed three times by acetonitrile and two times by ethanol using centrifugation (20000 rpm, 30 min).

The product, the nanosized FAU zeolite containing ruthenium complex (Ru(bpy)₃-FAU), is used as solid and colloidal suspension (distilled water as solvent) for further characterization.

Characterization

Dynamic light scattering (DLS) and zeta potential: The size of the nanoparticles in water suspension was measured by a Malvern Zetasizer Nano instrument using a backscattering geometry (scattering angle of 173°, He–Ne laser with a 3 mW output power at a wavelength of 632.8 nm). The DLS analyses were performed on water suspensions at a solid concentration of 1 wt %. The surface charge of the crystals was determined by measuring the zeta potential value of water suspensions at a constant solid concentration of 1 wt %.

X-ray diffraction (XRD): The crystallinity of the powder samples (FAU and Ru(bpy)₃-FAU) was evaluated using a *PANalytical*X'Pert Pro diffractometer with a CuK α monochromatized radiation ($\lambda = 1.5418 \text{ \AA}$).

N₂ adsorption: The porosity of the samples was measured using Micrometrics ASAP 2020 volumetric adsorption analyzer. Samples were degassed at 275 °C under vacuum overnight before the measurement. The external surface area and micropore volume were estimated by the alpha-plot method using Silica-1000 (22.1 m² g⁻¹ assumed) as a reference. The micropore and mesopore size distributions of solids were estimated by the Nonlocal Density Functional Theory (NLDFT) and Barret-Joyner-Halenda (BJH) methods using the desorption branch, respectively.

Thermogravimetric analysis (TGA): The amount of ruthenium-tris(2,2'-bipyridyl) and

moisture in the samples were investigated using SETSYS instrument (SETARAM) analyzer. Samples were heated with 5 °C min⁻¹ rate under 40 ml.min⁻¹ flow of air.

***In situ* Fourier Transform Infrared Spectroscopy (FTIR):** Zeolite powders were pressed (~10⁷ Pa) into self-supported disks (2 cm² area, 20 mg·cm⁻²) and placed in an IR cell equipped with KBr windows. IR spectra were recorded using a Nicolet 6700 IR spectrometer (Thermo Scientific, Villebon sur Yvette, France) equipped with a mercury cadmium telluride (MCT) detector and an extended KBr beam splitter. Spectra were recorded in the 400–5500 cm⁻¹ range at 4 cm⁻¹ with 128 scans. A homemade IR cell was used to evacuate the samples; then samples were heated up to 200 °C for 2 h under vacuum before the measurements. Various amounts of oxygen (0–100 Torr) and carbon dioxide (0–20 Torr) were introduced into the cell and kept in equilibrium for 5 min at -196 °C in the case of O₂, and for 1 min at room temperature in the case of CO₂ before recording each spectrum. The zeolites were loaded with increasing amounts of O₂ and CO₂ until their corresponding FTIR bands reached saturation. To allow the comparison of different samples, the spectra were normalized to the samples' mass and plotted as absorbance per gram over the wavelength

UV-vis absorption spectroscopy: The UV–vis absorption spectra of the zeolite suspensions were recorded on a Varian Cary 4000 UV–vis spectrometer in transmission mode using a quartz cuvette with a 1 cm path length. The as-synthesized zeolite (FAU) without Ru(bpy)₃ was used as a reference.

Excitation and luminescence study: The excitation and emission spectra of the diluted Ru(bpy)₃-X zeolite sample (50 µg/mL diluted 10x with dH₂O in 96-well plates) were recorded using Spark microplate reader (Tecan Group Ltd., Switzerland).

Cell culture: U251-MG (Sigma-Aldrich) human glioblastoma cells were cultured in Dulbecco's Modified Eagle Medium DMEM (1x) with 10% of Fetal Bovine Serum, 1% of Penicillin-Streptomycin, and 1% glutamin. The cell line was maintained under a humidified atmosphere containing 5% CO₂ at 37°C.

Cell viability assay: Crystal violet assay followed by spectrophotometric assay were performed to assess the effect of Ru(bpy)₃-FAU on cell viability. For this purpose, U251-MG cells were seeded into 96-well plates at the concentration of 7500 cells/well and incubated overnight at 37°C under 5% CO₂ atmosphere. Then the media was replaced by zeolite suspensions with increasing the concentrations of 50-100-250-500 µg/mL, and incubated for 1 day, 4 days and 7 days. At each time point, the culture medium was removed from wells and the plate was washed with warmed Phosphate Buffered Saline (PBS). Crystal violet dye solution (500 µL) was added into each well and the plate was incubated for 30 minutes at room temperature; the plate was washed with water and dried. The crystal violet dye was solubilized by adding 1 mL of 10 % acetic acid. The plate was agitated on orbital shaker until the color became uniform with no areas of dense coloration in the bottom of wells. The absorbance at 600 nm in a microplate reader was measured. In order to verify the density of the cells after staining, light microscopy images were taken by Nikon inverted microscope.

Confocal microscopy analysis: The cell uptake of Ru(bpy)₃-FAU into U251-MG cells was investigated by confocal microscopy. The cells were seeded onto coverslips in 24-well plates with a density of 2x10⁴ cells per well, and incubated at 37°C in 5% CO₂ atmosphere overnight. Afterwards, 50 µg/mL of the zeolite was added and incubated for 3 days. At the end of the incubation period, the cells were rinsed with PBS and fixed with 4% paraformaldehyde for 15

min. After washing with PBS, nuclei were stained with Hoechst 33342 (10 $\mu\text{g/ml}$) for 10 min. In the next step, the samples washed two times with PBS (5 min each) and the cells were mounted.

Confocal images with a 60x immersion oil objective were obtained with an Olympus FV1000 confocal microscope (Olympus). Excitation and emission spectra of markers Hoescht 361/497 nm, $\text{Ru}(\text{bpy})_3\text{-FAU}$ 488/543 nm. The images were edited using FV1000 software (Olympus) and Fiji/Image J.³⁴

Results and Discussion

Physicochemical characterization of nanosized $\text{Ru}(\text{bpy})_3\text{-FAU}$ zeolite

The structure and crystallinity of the as-synthesized and the modified FAU zeolite after encapsulating ruthenium-tris(2,2'-bipyridyl) are studied by X-ray diffraction. The XRD pattern of the $\text{Ru}(\text{bpy})_3\text{-FAU}$ zeolite perfectly matches that of the as-synthesized FAU zeolite (Figure 1). Moreover, the broad Bragg peaks recorded for both samples suggest the presence of zeolite crystals with small dimensions.

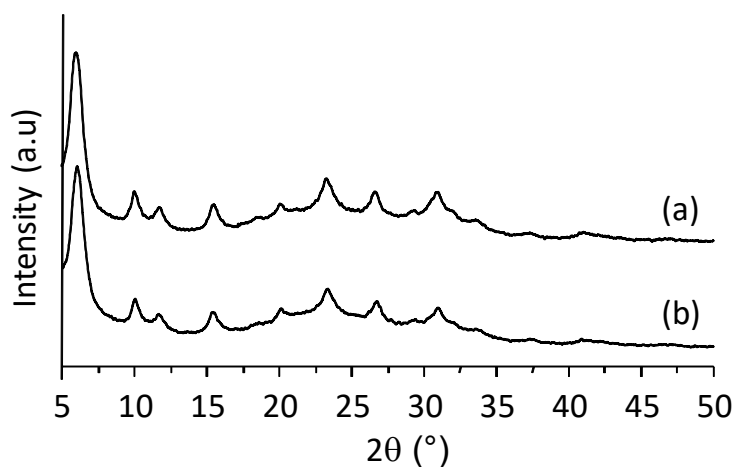


Figure 1. XRD patterns of (a) as-synthesized FAU and (b) $\text{Ru}(\text{bpy})_3\text{-FAU}$ zeolite samples.

The size of the crystals in the samples was further characterized by DLS (Figure 2A). Very small discrete crystals with an average size of 20-30 nm were unveiled; a monomodal particle size distribution curve was measured with no evidence of aggregation. Confining the ruthenium complex within the zeolite nanocrystals did not impact its stability in the colloidal suspensions using water as a solvent. The as-synthesized FAU and Ru(bpy)₃-FAU zeolite samples exhibited high negative zeta potential values of -51 mV and -42 mV, respectively that confirms the negative surface charge of the crystals and high stability (Figure 2B).

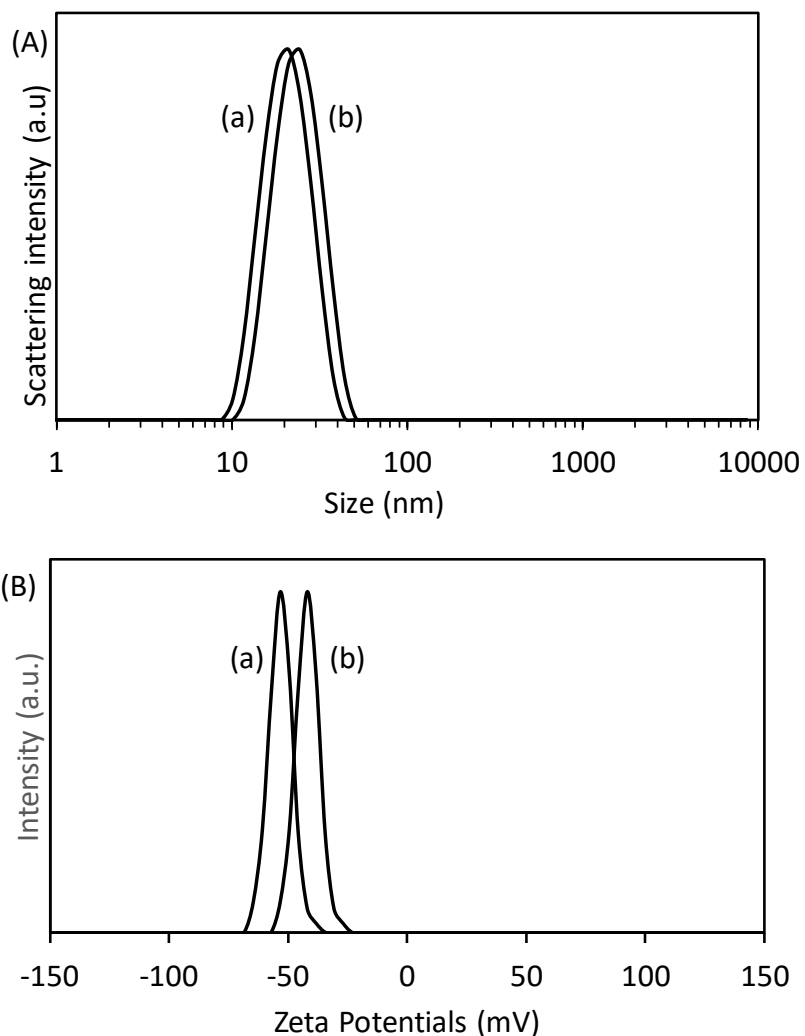


Figure 2. (A) Particle size distribution and (B) zeta potential curves of (a) as-synthesized FAU and (b) Ru(bpy)₃-FAU zeolite samples measured by Dynamic Light Scattering (DLS).

Thermogravimetric analyses (TGA) revealed that the as-prepared FAU zeolite loses 23% of its mass at 79 °C and 120 °C. These losses are attributed to the release of H₂O molecules from the surface and from the channels of the zeolite crystals (Figure 3). A different TG profile was recorded for the Ru(bpy)₃-FAU sample; a single mass loss at 120 °C was measured that

correspond to H₂O with lower quantity (17%) than the parent FAU sample. This decrease of water content can be explained by the partial replacement of water with the ruthenium complex. The ruthenium complex was released from the Ru(bpy)₃-FAU sample in the temperature range of 280-500 °C contributing to 8 % of the total mass loss (Figure 3). The ruthenium-tris(2,2'-bipyridyl) complex was eliminated from the zeolite in a step-wise manner exemplified by the appearance of 4 mass losses at high temperatures: two overlapping bands in the range of 280-350 °C, one band at 395 °C, and two partially overlapping bands at high temperature (470-500 °C) (Figure 3Aa and 3Ba). The presence of ruthenium-tris(2,2'-bipyridyl) is further confirmed by FTIR. The characteristic bands at 1600 (ν₂₅), 1486 (ν₁₈+ν₃₃), 1464 (ν₂₇), 1448 (ν₁₈+γCH), and 1427 cm⁻¹(ν₂₈) resembling those of bipyridyl ligand are present (Figure S1).³⁵

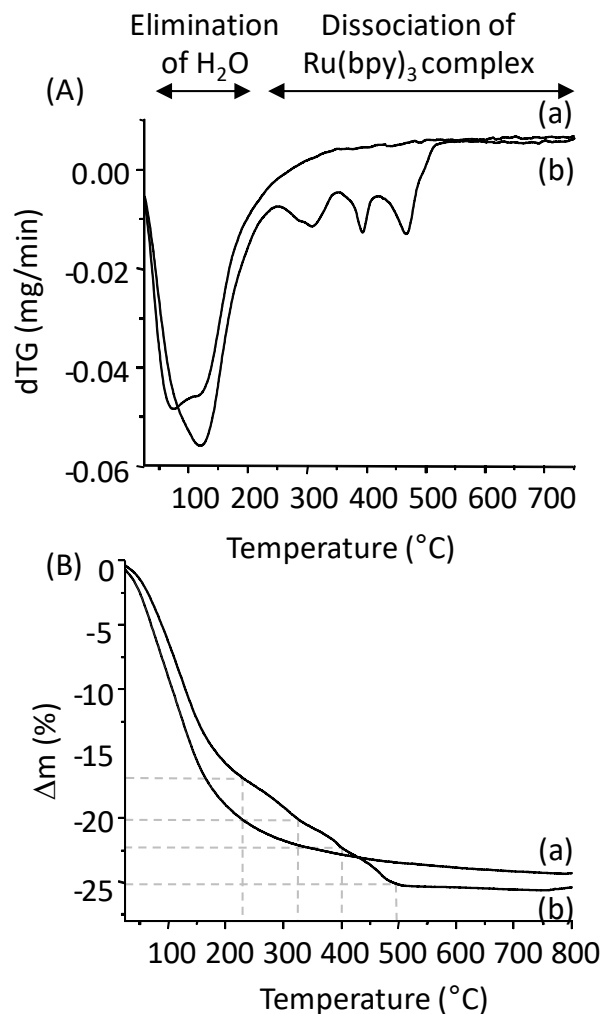


Figure 3. (A) Thermogravimetric (TG) analyses and (B) Differential thermogravimetric (dTG) of (a) as-prepared FAU and (b) Ru(bpy)₃-FAU samples.

The successful incorporation of the ruthenium complex in the FAU is also proved by N₂ sorption analyses (Figure 4). A remarkable decrease in BET specific surface area, S_{BET} (22%) and micropore volume (28 %) in comparison to the parent FAU zeolite was measured for the Ru(bpy)₃-FAU sample (Table 1). In contrast, a negligible decrease in the external surface area less than < 3 % was observed. These results indicate that the ruthenium complex is mainly

localized in the internal voids and can be occasionally found on the pore openings, but it is not present on the surface of FAU zeolite crystals.

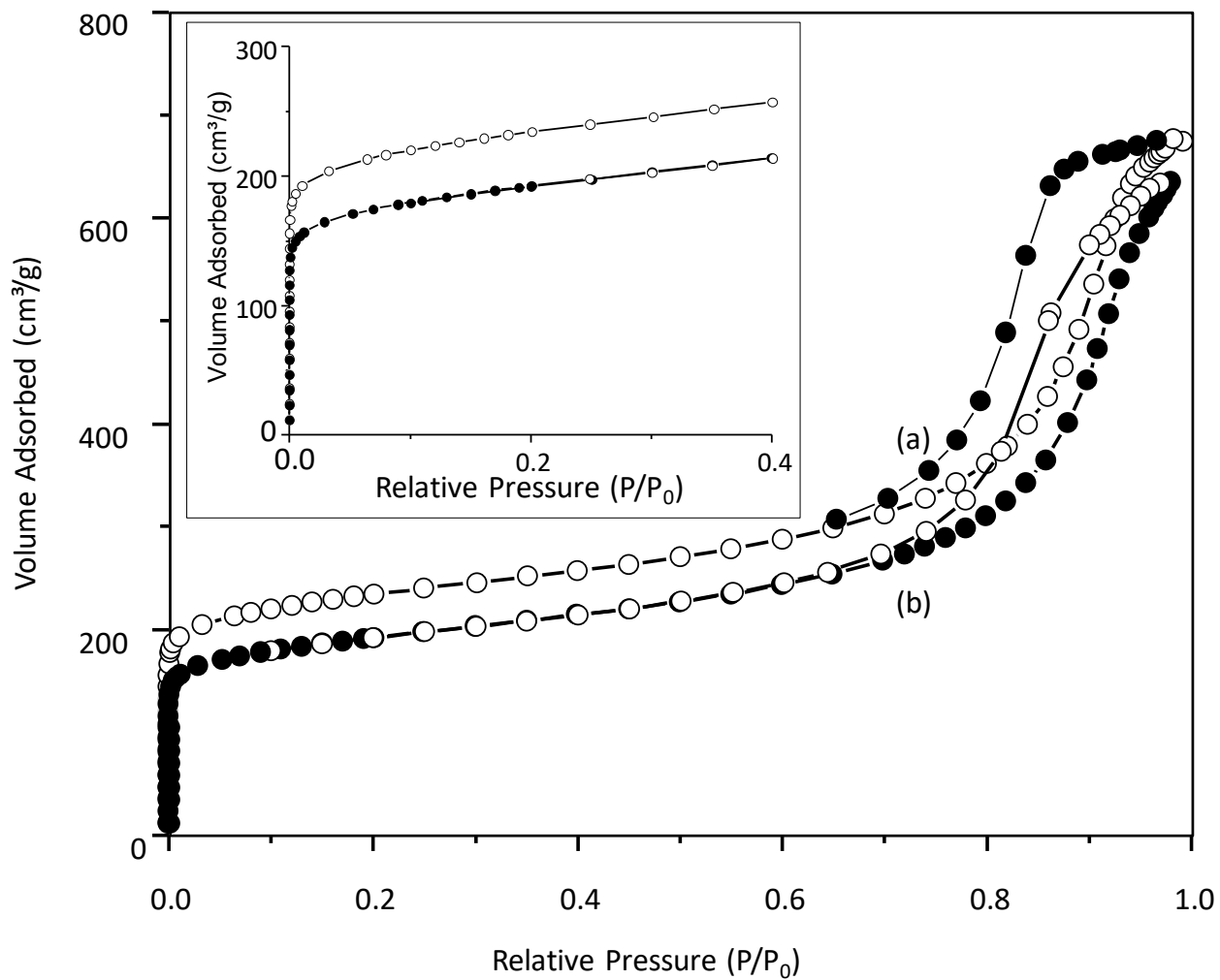


Figure 4. Nitrogen adsorption/desorption isotherms of (a) as-prepared FAU and (b) Ru(bpy)₃-FAU samples.

Table 1. Surface area and pore volume of as-prepared FAU and the Ru(bpy)₃-FAU samples determined by N₂ sorption measurements.

	S_{BET} ($\text{m}^2 \cdot \text{g}^{-1}$)	S_{Ext} ($\text{m}^2 \cdot \text{g}^{-1}$)	V_{mic} ($\text{cm}^3 \cdot \text{g}^{-1}$)	V_{mes} ($\text{cm}^3 \cdot \text{g}^{-1}$)	V_{total} ($\text{cm}^3 \cdot \text{g}^{-1}$)
FAU	760	278	0.28	0.72	1
Ru(bpy) ₃ -FAU	590	270	0.20	0.76	0.96

The incorporation of ruthenium-tris(2,2'-bipyridyl) complex in the Ru(bpy)₃-FAU zeolite sample was further validated by UV-vis spectroscopy (Figure 5A). A typical UV-vis spectrum of Ru(bpy)₃²⁺ was recorded which contains (i) an intense band at 285 nm attributed to the π - π^* ligand-center (LC) transitions, (ii) two shoulders around 325 and 345 nm corresponding to the d-d metal-centered (MC) transitions, and (iii) a band at 240 nm together with a broad band extending from 380 nm to 500 nm in the visible region attributed to the metal to ligand charge transfer (MLCT) transitions from the d-orbitals of the Ru metal center to the π^* orbitals of the pyridyl rings.³⁶⁻³⁹ Considering that the sample was thoroughly washed before the measurement, all non-reacted species or loosely adsorbed complexes are eliminated. Consequently, the recorded spectrum corresponds only to the species associated with the zeolite. The same absorption features were also recorded for the Ru(bpy)₃-FAU powder (Figure S2), thus confirming the association of these absorption features to the Ru(bpy)₃-FAU zeolite sample.

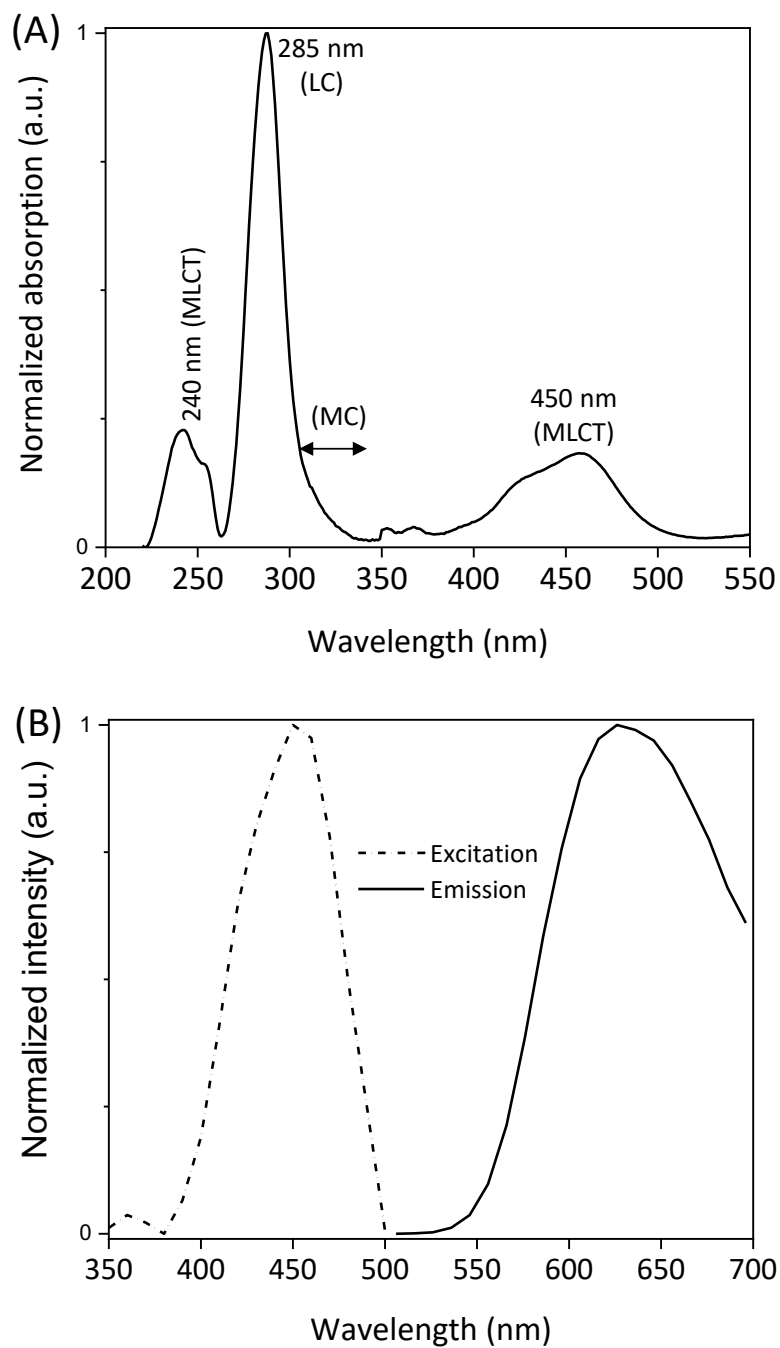


Figure 5. (A) UV-vis absorption spectrum, (B) excitation (dotted line) and emission (continuous line) spectra of Ru(bpy)₃-FAU sample.

The excitation spectrum of the sample Ru(bpy)₃-FAU shows a band centered at 450 nm (Figure 6B) resembling the MLCT band of the absorption profile (Figure 5A). This observation suggests that the low-lying MLCT is the emissive transition of the Ru(bpy)₃-FAU zeolite. Indeed, upon exciting at 450 nm, an orange-red emission at 628 nm is generated (Figure 5B). This emission is characterized by a structureless broad band, large Stokes shift from the excitation wavelength (~170 nm), and large redshift from the emission wavelength of the free bipyridine ligand (423 nm).³⁷ These findings confirm the attribution of luminescence to ³MLCT. Such feature permits the use of Ru(bpy)₃-FAU zeolite as an intracellular localization tracer agent in cellular imaging and for localizing the zeolite nanocrystals.

Further the CO₂ adsorption capacity of the as-prepared FAU and Ru(bpy)₃-FAU samples were studied by in situ FTIR spectroscopy. The CO₂ loaded in a carrier such as nanoparticles is highly desirable for controlled release into the vessels provoking blood dilatation. The FTIR spectra for both samples before and after delivery of CO₂ (1 Torr for FAU and 20 Torr for Ru(bpy)₃-FAU) are depicted in Figure S3. After the CO₂ adsorption, the spectra exhibit a new band at 2345 cm⁻¹ corresponding to physisorbed CO₂ and a set of bands in the region 1725 cm⁻¹ to 1350 cm⁻¹ associated with the chemisorbed CO₂ species. On the other hand, the chemisorbed CO₂ or carbonates are produced following the chemical interaction between the extra framework cations in the FAU zeolite and CO₂, these bonds are stable and cannot release CO₂ at the body temperature. The FTIR bands of the chemisorbed species partially overlap with those of the ruthenium complex, which prevents their accurate quantification.

Quantifying the physisorbed CO₂ via the FTIR band at 2345 cm⁻¹ revealed a higher tendency of Ru(bpy)₃-FAU towards CO₂ adsorption than FAU (Figure S4). More specifically, an increase in

CO₂ loading capacity of about 17 % was recorded for the Ru(bpy)₃-FAU compared to the as prepared FAU zeolite. Despite its higher CO₂ loading capacity, the adsorption on Ru(bpy)₃-FAU was slower than on the as-prepared FAU zeolite, this is exemplified by the lower slope of the curve representing the change of the FTIR band area versus the applied CO₂ pressure. This phenomenon is attributed to the partial obstruction of pores by the presence of ruthenium complex. The modified zeolite is capable of loading molecular oxygen, exemplified by the appearance of the band at 1552 cm⁻¹ following the O₂ adsorption experiment (Figure S5). The O₂ loading capacity of the Ru(bpy)₃-FAU sample was lower than that of the as-prepared FAU sample.

Nanosized Ru(bpy)₃-FAU zeolite as an intracellular localization tracer

To exploit the potential of Ru(bpy)₃-FAU zeolite nanoparticles as an intracellular localization tracer or in the future as a vector for delivery of either gases or drugs, the intracellular localization in U251-MG cells was determined. The U251-MG cells incubated with 50 µg/mL of zeolite nanoparticles for 4 h, 24 h and 72 h were studied by epifluorescent and confocal microscopy (Figure 6). After 4h of incubation, the Ru(bpy)₃-FAU zeolite nanocrystals are concentrated around the cells (Figure 6A). Upon increasing the incubation time, the particles started to cross the cell membrane and accumulate into the cytoplasm around the nucleus (Figure 6B and 6C). In this examination the green excitation was used. This filter encompass an excitation wavelength 510-580 nm and emission wavelength 620 nm which matches with emission maximum of the Ru(bpy)₃-FAU and naturally red color was obtained. The intracellular localization of the Ru(bpy)₃-FAU was studied by confocal microscopy. Figure 6D and 6E are the confocal micrographs of U251-MG cells after 72 h of incubation with the Ru(bpy)₃-FAU zeolite

(50 $\mu\text{g/mL}$). This observation was performed using blue excitation filter which covers excitation wavelength in the range of 420 - 495nm and emission wavelength at 535 nm. That set of filter and excitation maxima of $\text{Ru}(\text{bpy})_3\text{-FAU}$ (450nm) allows us to obtain green signal. After 72 h, a significant amount of $\text{Ru}(\text{bpy})_3\text{-FAU}$ zeolite nanoparticles was predominantly localized around the nucleus and at much lesser extent, on the nucleus (Figure 6D). The orthogonal view was obtained following z-stacking of the region which was marked with red-dashed circle. Figure (6E) revealed that a small amount of particles entered into the nucleus.

Figure 6. Epifluorescent (A, B, C) and confocal microscopy images (D, E) showing the uptake of $\text{Ru}(\text{bpy})_3\text{-FAU}$ zeolite by U-251-MG cells. (A) (B) and (C) represent progressive uptake of the tracer molecule. (D) The top and magnified orthogonal view (E) of the U251-MG cells. Yellow and red arrows show cytoplasmic and intranuclear deposition of $\text{Ru}(\text{bpy})_3\text{-FAU}$, respectively.

Our results are in line with the previous study demonstrating that small- nanoparticles (25 nm) show higher nuclear delivery to gain nuclear entry in a passive manner.⁴⁰ In addition to that, the shape and size of particles was shown to have an influence on the uptake process by the cells.^{41,42} The optimal nanoparticle radius for endocytosis was previously determined to be in the range of 25–30 nm,⁴² which is in a good agreement with prior estimates.⁴³ The current results are also in an agreement with other studies reported that nanoparticles with a size of 50 nm and 120 nm are internalized faster in comparison to 250 nm particles.⁴⁴ In a very recent study,⁴⁵ the kinetics of uptake of zeolite L and NaY by Hs 578T breast cancer cells and MCF-10 epithelial mammary cells was presented. The NaY zeolite had cubic geometry with an average diameter of 700 nm, while zeolite L had disc-shaped particles with a size of around 400 nm. The cells started to engulf the NY particles with their filopodia, but only a few of them were inside the cell due to the big size and formation of aggregates. However, after 5 min of incubation more L zeolite particles were internalized than zeolite NaY.

It is also known that in addition to the size and shape, the surface charge of the particles have an impact on internalization efficacy. The surface functionalization of nanoparticles can be utilized to promote cellular uptake and determine nanoparticle sub-cellular localization. The most frequently postulated internalization pathway is endocytosis. However, the exact mechanism has been shown to be cell-type dependent. The cell nucleus intuitively becomes of primary interest for targeting nanoparticles and also has been proven to be the main interaction site for most therapeutic agents such as anticancer drugs, genes, free radicals, and heat.

Toxicity study of Ru(bpy)₃-FAU zeolite nanoparticles

In vitro cytocompatibility of Ru(bpy)₃-FAU zeolite nanoparticles on U251-MG cells was tested by crystal violet assay. Adherent cells detach from cell culture plates during the cell death. The difference in proliferation upon treatment with test agent is used for indirect quantification of cell death. In other words, cells that undergo cell death lose their adherence and are subsequently lost from the population of cells, reducing the amount of crystal violet staining in a culture.

U251-MG cells were treated with increased concentrations of Ru(bpy)₃-FAU zeolite nanoparticles (50, 100, 250 and 500 µg/mL), and viability was followed at Days 1, 4 and 7 (Figure 7). The effects of Ru(bpy)₃-FAU zeolite nanoparticles on the cell growth was also shown by light microscopy images (Figure 7A). The density of the cells were relatively similar after 1 day of exposure. However, the number of the cells has decreased upon exposure to 50 and 100 µg/mL Ru(bpy)₃-FAU zeolite nanoparticles after 4 days. Although the cells started to recover from the inhibitory effect of Ru(bpy)₃-FAU and continue to proliferate along 7 days, concentration dependent slight decrease was observed.

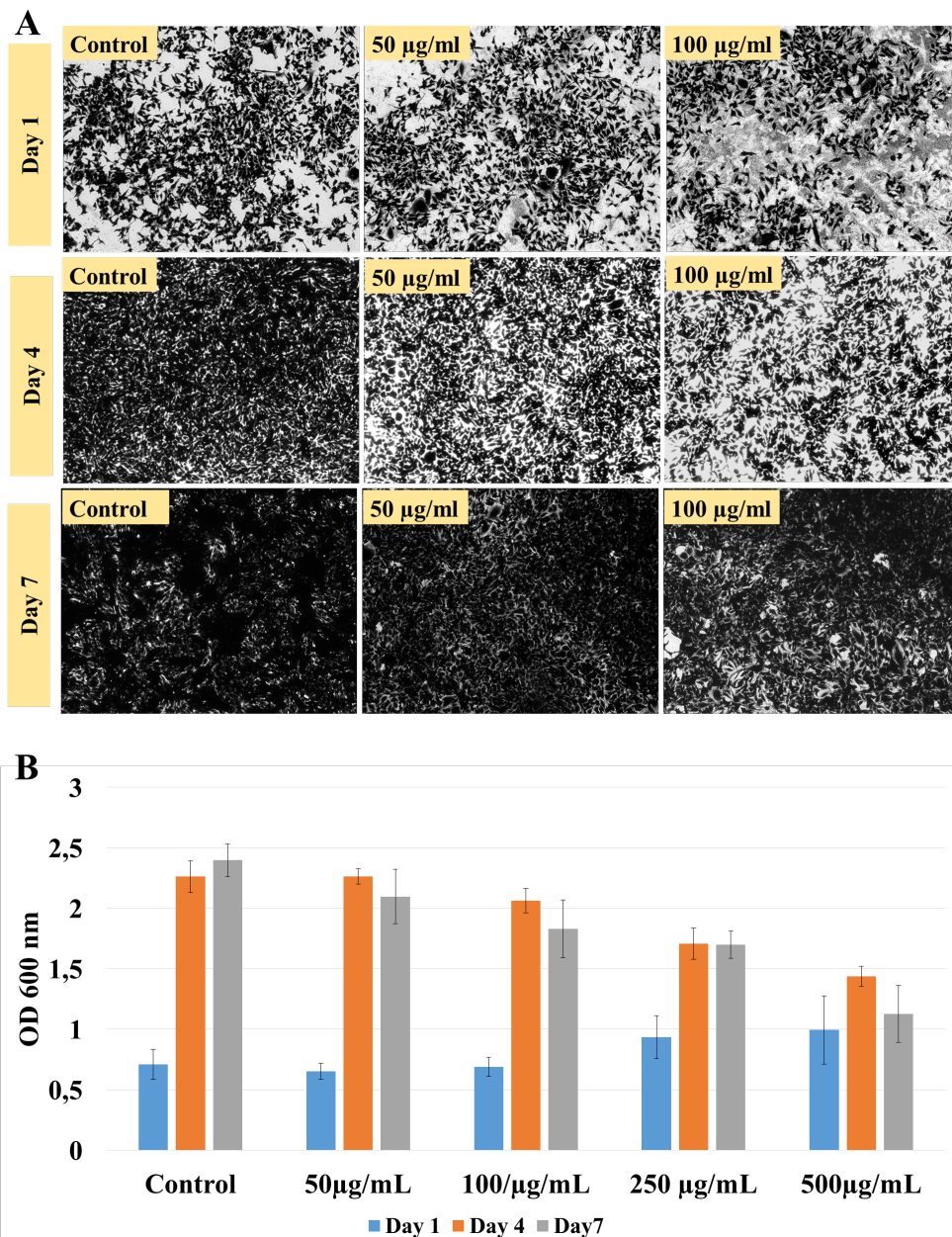


Figure 7. (A) Light microscopy images of U251-MG cells after crystal violet staining after 1 day, 4 and 7 days exposure to Ru(bpy)₃-FAU zeolite. (B) The viability of human glioblastoma cells after 1 day, 4 and 7 days exposure to Ru(bpy)₃-FAU zeolite samples with different concentrations (50,100, 250 and 500 µg/mL).

To further confirm these observations, the viability of the cells was quantified by measuring optical density following crystal violet staining (Figure 7B). After one day of exposure, in the range of the tested concentrations, the zeolite nanoparticles did not exhibit toxicity to the cells as confirmed by the stability (even a slight increase) in optical density. Ru(bpy)₃-FAU showed concentration dependent decrease in the viability of U251-MG cells at Days 4 and 7 in a concentration dependent manner. However, the lethal dose 50% was not achieved even working with the highest concentration of Ru(bpy)₃-FAU nanoparticles (500µg/ml) We can conclude that the Ru(bpy)₃-FAU zeolite nanoparticles are safe for these cells. While using silver-containing zeolites even with low concentrations (as low as 50µg/ml)³ no cells survived after 24 or 48 exposure was registered.³

Conclusions

We successfully incorporated ruthenium-tris(2,2'-bipyridyl) complex within FAU zeolite nanocrystals. The FAU nanocrystals were loaded with 8 % ruthenium-tris(2,2'-bipyridyl). The introduction of this complex in the zeolite crystals did not change the morphology, crystallinity, and colloidal stability of the sample.

The ruthenium-tris(2,2'-bipyridyl) complex introduced in the FAU zeolite retained its absorption properties. Upon excitation at the MLCT band at 450 nm, an orange-red emission appeared at 628 nm, typical for organometallic complexes bearing π -conjugated ligands which is not common for pure zeolite.

The viability tests were performed revealing the concentration and time dependent toxicity of the Ru(bpy)₃-FAU zeolite on U251 cells. The safest dose range of the Ru(bpy)₃-FAU nanoparticles was in the range of 50-100 µg/mL. Furthermore, confocal microscopy imaging show the internalization of the zeolite nanocrystals in the cells owing to their luminescent properties inherited from the ruthenium complex. The Ru(bpy)₃-FAU was shown to be able of crossing the cell membrane barrier and localized mostly at the perinuclear regions with some intranuclear uptake.

Being stable, safe, capable of loading various guest molecules (drugs and gases) and instantaneously localized within the cells, the Ru(bpy)₃-FAU nanosized zeolite crystals could be considered as a potential candidate for medical application.

Acknowledgement

The financial support provided by ZEOXY project (Conseil Régional de Basse Normandie) and the European Union-Fonds Européen de Développement Régional (FEDER) is acknowledged.

The authors thank the Institut National du Cancer (INCA-11699).

References

- (1) Zaarour, M.; Dong, B.; Naydenova, I.; Retoux, R.; Mintova, S. Progress in Zeolite Synthesis Promotes Advanced Applications. *Microporous Mesoporous Mater.* **2014**, *189*, 11–21.
<https://doi.org/10.1016/j.micromeso.2013.08.014>.
- (2) Bacakova, L.; Vandrovцова, M.; Kopova, I.; Jirka, I. Applications of Zeolites in Biotechnology and Medicine – a Review. *Biomater. Sci.* **2018**, *6* (5), 974–989.

<https://doi.org/10.1039/C8BM00028J>.

- (3) Anfray, C.; Dong, B.; Komaty, S.; Mintova, S.; Valable, S. Acute Toxicity of Silver Free and Encapsulated in Nanosized Zeolite for Eukaryotic Cells. *ACS Appl. Mater. Interfaces* **2017**, *9* (16), 13849–13854. <https://doi.org/10.1021/acsami.7b00265>.
- (4) Dong, B.; Belkhair, S.; Zaarour, M.; Fisher, L.; Verran, J.; Tosheva, L.; Retoux, R.; Gilson, J. P.; Mintova, S. Silver Confined within Zeolite EMT Nanoparticles: Preparation and Antibacterial Properties. *Nanoscale* **2014**, *6* (18), 10859–10864. <https://doi.org/10.1039/c4nr03169e>.
- (5) Vilaça, N.; Amorim, R.; Machado, A. F.; Parpot, P.; Pereira, M. F. R.; Sardo, M.; Rocha, J.; Fonseca, A. M.; Neves, I. C.; Baltazar, F. Potentiation of 5-Fluorouracil Encapsulated in Zeolites as Drug Delivery Systems for in Vitro Models of Colorectal Carcinoma. *Colloids Surfaces B Biointerfaces* **2013**, *112*, 237–244. <https://doi.org/10.1016/j.colsurfb.2013.07.042>.
- (6) Seifu, D. G.; Isimjan, T. T.; Mequanint, K. Tissue Engineering Scaffolds Containing Embedded Fluorinated-Zeolite Oxygen Vectors. *Acta Biomater.* **2011**, *7* (10), 3670–3678. <https://doi.org/10.1016/j.actbio.2011.06.010>.
- (7) Komaty, S.; Anfray, C.; Zaarour, M.; Awala, H.; Ruaux, V.; Valable, S.; Mintova, S. A Facile Route toward the Increase of Oxygen Content in Nanosized Zeolite by Insertion of Cerium and Fluorinated Compounds. *Molecules* **2018**, *23* (2), 37. <https://doi.org/10.3390/molecules23020037>.
- (8) Tavolaro, A.; Tavolaro, P.; Drioli, E. Zeolite Inorganic Supports for BSA Immobilization: Comparative Study of Several Zeolite Crystals and Composite Membranes. *Colloids Surf. B. Biointerfaces* **2007**, *55* (1), 67–76. <https://doi.org/10.1016/j.colsurfb.2006.11.010>.
- (9) Datt, A.; Burns, E. A.; Dhuna, N. A.; Larsen, S. C. Loading and Release of 5-Fluorouracil from HY Zeolites with Varying SiO₂/Al₂O₃ Ratios. *Microporous Mesoporous Mater.* **2013**, *167*, 182–

187. <https://doi.org/10.1016/j.micromeso.2012.09.011>.
- (10) Spanakis, M.; Bouropoulos, N.; Theodoropoulos, D.; Sygellou, L.; Ewart, S.; Moschovi, A. M.; Siokou, A.; Niopas, I.; Kachrimanis, K.; Nikolakis, V.; et al. Controlled Release of 5-Fluorouracil from Microporous Zeolites. *Nanomedicine Nanotechnology, Biol. Med.* **2014**, *10* (1), 197–205. <https://doi.org/10.1016/j.nano.2013.06.016>.
- (11) Grund, S.; Doussineau, T.; Fischer, D.; Mohr, G. J. Mitoxantrone-Loaded Zeolite Beta Nanoparticles: Preparation, Physico-Chemical Characterization and Biological Evaluation. *J. Colloid Interface Sci.* **2012**, *365* (1), 33–40. <https://doi.org/10.1016/j.jcis.2011.09.003>.
- (12) Lülff, H.; Bertucci, A.; Septiadi, D.; Corradini, R.; De Cola, L. Multifunctional Inorganic Nanocontainers for DNA and Drug Delivery into Living Cells. *Chem. - A Eur. J.* **2014**, *20* (35), 10900–10904. <https://doi.org/10.1002/chem.201403232>.
- (13) Bertucci, A.; Lülff, H.; Septiadi, D.; Manicardi, A.; Corradini, R.; De Cola, L. Intracellular Delivery of Peptide Nucleic Acid and Organic Molecules Using Zeolite-L Nanocrystals. *Adv. Healthc. Mater.* **2014**, *3* (11), 1812–1817. <https://doi.org/10.1002/adhm.201400116>.
- (14) Fatouros, D. G.; Douroumis, D.; Nikolakis, V.; Ntais, S.; Moschovi, A. M.; Trivedi, V.; Khima, B.; Roldo, M.; Nazar, H.; Cox, P. A. In Vitro and in Silico Investigations of Drug Delivery via Zeolite BEA. *J. Mater. Chem.* **2011**, *21* (21), 7789–7794. <https://doi.org/10.1039/c1jm10204d>.
- (15) Paradee, N.; Sirivat, A. Encapsulation of Folic Acid in Zeolite y for Controlled Release via Electric Field. *Mol. Pharm.* **2016**, *13* (1), 155–162. <https://doi.org/10.1021/acs.molpharmaceut.5b00592>.
- (16) Karavasili, C.; Kokove, L.; Kontopoulou, I.; Eleftheriadis, G. K.; Bouropoulos, N.; Fatouros, D. G. Dissolution Enhancement of the Poorly Soluble Drug Nifedipine by Co-Spray Drying with

- Microporous Zeolite Beta. *J. Drug Deliv. Sci. Technol.* **2016**, *35*, 91–97.
<https://doi.org/10.1016/j.jddst.2016.06.004>.
- (17) Karavasili, C.; Amanatiadou, E. P.; Kontogiannidou, E.; Eleftheriadis, G. K.; Bouropoulos, N.; Pavlidou, E.; Kontopoulou, I.; Vizirianakis, I. S.; Fatouros, D. G. Comparison of Different Zeolite Framework Types as Carriers for the Oral Delivery of the Poorly Soluble Drug Indomethacin. *Int. J. Pharm.* **2017**, *528* (1–2), 76–87. <https://doi.org/10.1016/j.ijpharm.2017.05.061>.
- (18) Komaty, S.; Daouli, A.; Badawi, M.; Anfray, C.; Zaarour, M.; Valable, S.; Mintova, S. Incorporation of Trivalent Cations in NaX Zeolite Nanocrystals for the Adsorption of O₂ in the Presence of CO₂. *Phys. Chem. Chem. Phys.* **2020**. <https://doi.org/10.1039/D0CP00111B>.
- (19) Braschi, I.; Blasioli, S.; Gigli, L.; Gessa, C. E.; Alberti, A.; Martucci, A. Removal of Sulfonamide Antibiotics from Water: Evidence of Adsorption into an Organophilic Zeolite Y by Its Structural Modifications. *J. Hazard. Mater.* **2010**, *178* (1–3), 218–225.
<https://doi.org/10.1016/j.jhazmat.2010.01.066>.
- (20) Zhang, H.; Kim, Y.; Dutta, P. K. Controlled Release of Paraquat from Surface-Modified Zeolite Y. *Microporous Mesoporous Mater.* **2006**, *88* (1–3), 312–318.
<https://doi.org/10.1016/j.micromeso.2005.09.026>.
- (21) Dong, B.; Retoux, R.; de Waele, V.; Chiodo, S. G.; Mineva, T.; Cardin, J.; Mintova, S. Sodalite Cages of EMT Zeolite Confined Neutral Molecular-like Silver Clusters. *Microporous Mesoporous Mater.* **2017**, *244*, 74–82. <https://doi.org/10.1016/j.micromeso.2017.02.029>.
- (22) Wang, Y.; Li, H. Luminescent Materials of Zeolite Functionalized with Lanthanides. *CrystEngComm* **2014**, *16* (42), 9764–9778. <https://doi.org/10.1039/C4CE01455C>.
- (23) Ruda-Eberenz, T. A.; Nagy, A.; Waldman, W. J.; Dutta, P. K. Entrapment of Ionic Tris(2,2'-

- Bipyridyl) Ruthenium(II) in Hydrophobic Siliceous Zeolite: O₂ Sensing in Biological Environments. *Langmuir* **2008**, *24* (16), 9140–9147. <https://doi.org/10.1021/la801204y>.
- (24) Busby, M.; Devaux, A.; Blum, C.; Subramaniam, V.; Calzaferri, G.; De Cola, L. Interactions of Perylene Bisimide in the One-Dimensional Channels of Zeolite L. *J. Phys. Chem. C* **2011**, *115* (13), 5974–5988. <https://doi.org/10.1021/jp1108625>.
- (25) Calzaferri, G.; Huber, S.; Maas, H.; Minkowski, C. Host-Guest Antenna Materials. *Angew. Chemie - Int. Ed.* **2003**, *42* (32), 3732–3758. <https://doi.org/10.1002/anie.200300570>.
- (26) Alarcos, N.; Cohen, B.; Ziólek, M.; Douhal, A. Photochemistry and Photophysics in Silica-Based Materials: Ultrafast and Single Molecule Spectroscopy Observation. *Chem. Rev.* **2017**, *117* (22), 13639–13720. <https://doi.org/10.1021/acs.chemrev.7b00422>.
- (27) Iversen, T.-G.; Skotland, T.; Sandvig, K. Endocytosis and Intracellular Transport of Nanoparticles: Present Knowledge and Need for Future Studies. *Nano Today* **2011**, *6* (2), 176–185. <https://doi.org/10.1016/j.nantod.2011.02.003>.
- (28) Sahay, G.; Alakhova, D. Y.; Kabanov, A. V. Endocytosis of Nanomedicines. *J. Control. Release* **2010**, *145* (3), 182–195. <https://doi.org/10.1016/j.jconrel.2010.01.036>.
- (29) Snipstad, S.; Hak, S.; Baghirov, H.; Sulheim, E.; Mørch, Ý.; Lélú, S.; von Haartman, E.; Bäck, M.; Nilsson, K. P. R.; Klymchenko, A. S.; et al. Labeling Nanoparticles: Dye Leakage and Altered Cellular Uptake. *Cytom. Part A* **2017**, *91* (8), 760–766. <https://doi.org/10.1002/cyto.a.22853>.
- (30) Payra, P.; Dutta, P. K. Development of a Dissolved Oxygen Sensor Using Tris(Bipyridyl) Ruthenium (II) Complexes Entrapped in Highly Siliceous Zeolites. *Microporous Mesoporous Mater.* **2003**, *64* (1–3), 109–118. <https://doi.org/10.1016/j.micromeso.2003.06.002>.
- (31) Meier, B.; Werner, T.; Klimant, I.; Wolfbeis, O. S. Novel Oxygen Sensor Material Based on a

- Ruthenium Bipyridyl Complex Encapsulated in Zeolite Y: Dramatic Differences in the Efficiency of Luminescence Quenching by Oxygen on Going from Surface-Adsorbed to Zeolite-Encapsulated Fluorophores. *Sensors Actuators B. Chem.* **1995**, *29* (1–3), 240–245. [https://doi.org/10.1016/0925-4005\(95\)01689-9](https://doi.org/10.1016/0925-4005(95)01689-9).
- (32) Coutant, M. A.; Payra, P. P.; Dutta, P. K. Oxygen Transport in Zeolite Y Measured by Quenching of Encapsulated Tris(Bipyridyl)Ruthenium. *Microporous Mesoporous Mater.* **2003**, *60* (1–3), 79–90. [https://doi.org/10.1016/S1387-1811\(03\)00327-5](https://doi.org/10.1016/S1387-1811(03)00327-5).
- (33) Awala, H.; Gilson, J. P.; Retoux, R.; Boullay, P.; Goupil, J. M.; Valtchev, V.; Mintova, S. Template-Free Nanosized Faujasite-Type Zeolites. *Nat. Mater.* **2015**, *14* (4), 447–451. <https://doi.org/10.1038/nmat4173>.
- (34) Rueden, C. T.; Schindelin, J.; Hiner, M. C.; DeZonia, B. E.; Walter, A. E.; Arena, E. T.; Eliceiri, K. W. ImageJ2: ImageJ for the next Generation of Scientific Image Data. *BMC Bioinformatics* **2017**, *18* (1), 529. <https://doi.org/10.1186/s12859-017-1934-z>.
- (35) Omberg, K. M.; Schoonover, J. R.; Treadway, J. A.; Leasure, R. M.; Brian Dyer, R.; Meyer, T. J. Mid-Infrared Spectrum of [Ru(Bpy)₃]²⁺. *J. Am. Chem. Soc.* **1997**, *119* (30), 7013–7018. <https://doi.org/10.1021/ja970511u>.
- (36) Kober, E. M.; Meyer, T. J. Concerning the Absorption Spectra of the Ions M(Bpy)₃²⁺ (M = Fe, Ru, Os; Bpy = 2,2'-Bipyridine). *Inorg. Chem.* **1982**, *21* (11), 3967–3977. <https://doi.org/10.1021/ic00141a021>.
- (37) Juris, A.; Balzani, V.; Barigelletti, F.; Campagna, S.; Belser, P.; von Zelewsky, A. Ru(II) Polypyridine Complexes: Photophysics, Photochemistry, Electrochemistry, and Chemiluminescence. *Coord. Chem. Rev.* **1988**, *84*, 85–277. [https://doi.org/10.1016/0010-8545\(88\)80032-8](https://doi.org/10.1016/0010-8545(88)80032-8).

- (38) Kalyanasundaram, K. Photophysics, Photochemistry and Solar Energy Conversion with Tris(Bipyridyl)Ruthenium(II) and Its Analogues. *Coord. Chem. Rev.* **1982**, *46* (C), 159–244. [https://doi.org/10.1016/0010-8545\(82\)85003-0](https://doi.org/10.1016/0010-8545(82)85003-0).
- (39) Kirketerp, M.-B. S.; Nielsen, S. B. Absorption Spectrum of Isolated Tris(2,2'-Bipyridine)Ruthenium(II) Dications in Vacuo. *Int. J. Mass Spectrom.* **2010**, *297* (1–3), 63–66. <https://doi.org/10.1016/j.ijms.2010.05.019>.
- (40) Tammam, S. N.; Azzazy, H. M. E.; Lamprecht, A. The Effect of Nanoparticle Size and NLS Density on Nuclear Targeting in Cancer and Normal Cells; Impaired Nuclear Import and Aberrant Nanoparticle Intracellular Trafficking in Glioma. *J. Control. Release* **2017**, *253*, 30–36. <https://doi.org/10.1016/j.jconrel.2017.02.029>.
- (41) Cho, E. C.; Au, L.; Zhang, Q.; Xia, Y. The Effects of Size, Shape, and Surface Functional Group of Gold Nanostructures on Their Adsorption and Internalization by Cells. *Small* **2010**, *6* (4), 517–522. <https://doi.org/10.1002/smll.200901622>.
- (42) Zhang, S.; Li, J.; Lykotrafitis, G.; Bao, G.; Suresh, S. Size-Dependent Endocytosis of Nanoparticles. *Adv. Mater.* **2009**, *21* (4), 419–424. <https://doi.org/10.1002/adma.200801393>.
- (43) Gao, H.; Shi, W.; Freund, L. B. Mechanics of Receptor-Mediated Endocytosis. *Proc. Natl. Acad. Sci.* **2005**, *102* (27), 9469–9474. <https://doi.org/10.1073/pnas.0503879102>.
- (44) Suen, W. L. L.; Chau, Y. Size-Dependent Internalisation of Folate-Decorated Nanoparticles via the Pathways of Clathrin and Caveolae-Mediated Endocytosis in ARPE-19 Cells. *J. Pharm. Pharmacol.* **2014**, *66* (4), 564–573. <https://doi.org/10.1111/jphp.12134>.
- (45) Vilaça, N.; Totovao, R.; Prasetyanto, E. A.; Miranda-Gonçalves, V.; Morais-Santos, F.; Fernandes, R.; Figueiredo, F.; Bañobre-López, M.; Fonseca, A. M.; De Cola, L.; et al. Internalization Studies

on Zeolite Nanoparticles Using Human Cells. *J. Mater. Chem. B* **2018**, 6 (3), 469–476.

<https://doi.org/10.1039/C7TB02534C>.